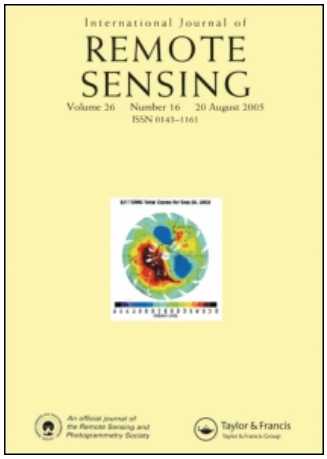

International Journal of Remote Sensing
Publication details, including instructions for authors and subscription information:
http://www.informaworld.com/smpp/title~content=t713722504

Mapping the height and above-ground biomass of a mixed forest using lidar and stereo Ikonos images

B. St-Onge [a]; Y. Hu [a]; C. Vega [b]

[a] Geography Department, Université du Québec à Montréal, Montréal, QC, Canada, H3C 3P8

[b] UMR TETIS Cemagref-Ciraz-Engref, Maison de la Télédétection en Languedoc-Roussillon, Montpellier Cedex 05, France

Online Publication Date: 01 March 2008

To cite this Article: St-Onge, B., Hu, Y. and Vega, C. (2008) 'Mapping the height and above-ground biomass of a mixed forest using lidar and stereo Ikonos images', International Journal of Remote Sensing, 29:5, 1277 — 1294

To link to this article: DOI: 10.1080/01431160701736505
URL: http://dx.doi.org/10.1080/01431160701736505

International Journal of Remote Sensing
Vol. 29, No. 5, 10 March 2008, 1277–1294

Mapping the height and above-ground biomass of a mixed forest using lidar and stereo Ikonos images

B. ST-ONGE*†, Y. HU† and C. VEGA‡
†Geography Department, Université du Québec à Montréal, Montréal, QC, Canada, H3C 3P8
‡UMR TETIS Cemagref-Ciraz-Engref, Maison de la Télédétction en Languedoc–Roussillon, Montpellier Cedex 05, France

Our objective was to assess the accuracy of the forest height and biomass estimates derived from an Ikonos stereo pair and a lidar digital terrain model (DTM). After the Ikonos scenes were registered to the DTM with submetric accuracy, tree heights were measured individually by subtracting the photogrammetric elevation of the treetop from the lidar ground-level elevation of the tree base. The low residual error (1.66 m) of the measurements confirmed the joint geometric accuracy of the combined models. Matched images of the stereo pair were then used to create a digital surface model. The latter was transformed to a canopy height model (CHM) by subtracting the lidar DTM. Plotwise height percentiles were extracted from the Ikonos-lidar CHM and used to predict the average dominant height and above-ground biomass. The coefficient of determination reached 0.91 and 0.79 for average height and biomass, respectively. In both cases, the accuracy of the Ikonos-lidar CHM predictions was slightly lower than that of the all-lidar reference CHM. Although the CHM heights did not saturate at moderate biomass levels, as do multispectral or radar images, values above 300 Mg ha^{-1} could not be predicted accurately by the Ikonos-lidar or by the all-lidar CHM.

1. Introduction

The quantification, mapping, and monitoring of forest biomass are now central issues of climate modelling due to their importance in the calculation of net carbon emissions (Kurz and Apps 2006). The assessment of biomass, or of the closely linked variable of timber volume, is also critical in forest management. However, practical or methodological limitations still restrict our capacity of producing accurate and spatially explicit estimates of forest biomass for large portions of land (Lu 2006). Because field sampling is onerous and limited to accessible areas, many researchers turned to remote sensing approaches for mapping biomass. These can be divided into two categories: (1) radiance-based predictive models that rely on the reflective characteristics of tree foliage in the visible, infrared or microwave bands (e.g. Santos *et al.* 2002, Austin *et al.* 2003, Zheng *et al.* 2004, Lu 2005) and (2) 3D reconstruction techniques such as IFSAR (InterFerometric Synthetic Aperture Radar), lidar (Light Detection and Ranging) or stereo-photogrammetry that attempt to directly quantify the vertical structure of canopies (e.g. Lim *et al.* 2002, Treuhaft and Siqueira 2004, Zagalikis *et al.* 2005). Although the methods from the first category are fairly

*Corresponding author. Email: st-onge.benoit@uqam.ca

International Journal of Remote Sensing
ISSN 0143-1161 print/ISSN 1366-5901 online
http://www.tandf.co.uk/journals
DOI: 10.1080/01431160701736505

effective for certain situations, such as young forests, they have the following persisting limitations: they require radiometric calibration to remove atmospheric and topographic effects, their predictive capacity saturates at relatively low biomass values (around 150–200 $Mg\,ha^{-1}$), and their transferability from scene to scene is difficult due to their sensitivity to environmental or acquisition conditions such as the sun or view angle, the phenological state of the vegetation, or variations in the spectral reflectance of the understorey (see reviews by Baltzer 2001 and Lu 2006 that provide several examples of these limitations). Conversely, the approaches from the second category, the 3D reconstruction techniques, exploit the strong relationship between canopy height and biomass. In northern mid- and high-latitude forests, this relationship is such that height can be used as a proxy for biomass (Fang *et al.* 2006). Scanning laser altimetry, hereafter termed 'lidar', currently appears to be one of the most accurate remote sensing techniques for estimating the height of individual trees or the average height of canopies (Hyyppä *et al.* 2001). Typically, lidar height distribution metrics within plots or stands are regressed against corresponding field reference data to build predictive models for height or biomass (Næsset 2002, Lim *et al.* 2003, Patenaude *et al.* 2004). These models can then be used to map such attributes over significant areas. Theoretically, this approach can be applied to any dataset from which height can be calculated by subtracting ground from canopy surface elevations. Potential alternatives to lidar include IFSAR (Treuhaft and Siqueira 2004), stereo-photogrammetry (Halbritter 2000, Miller *et al.* 2000, Zagalikis *et al.* 2005) or a combination of these to lidar (Andersen *et al.* 2003, St-Onge *et al.* 2004). We recently demonstrated that subtracting a lidar digital terrain model (DTM) from a digital surface model (DSM) extracted from stereo aerial photographs using image-matching techniques results in a canopy height model (CHM) that is very similar to its all-lidar equivalent (St-Onge and Véga 2003, St-Onge *et al.* 2006). However, in the case where biomass or volume needs to be mapped over areas of several hundred square kilometres on a regular basis, repeated lidar surveys might be too onerous. Moreover, the processing of blocks comprising a very large number of aerial photographs remains cumbersome. Finally, few providers offer aerial IFSAR surveys, and the resulting data are of variable quality as they are sometimes influenced by wind or vegetation wetness (Baltzer 2001). For relatively wide areas, high-resolution satellite stereo imagery could potentially be used instead of large- or medium-scale aerial photographs to produce DSMs. By subtracting the ground elevations obtained from archived lidar DTMs, CHMs could be efficiently produced. This is made possible by the rapidly growing coverage of lidar DTMs, the general stability of terrain elevations over time, and the high geometric accuracy of satellite linear array scanners such as Ikonos and QuickBird. The photogrammetric utility and quality of these two sensors were recently demonstrated by several authors. For both, high horizontal and vertical accuracies were achieved in image-to-object coordinate transformations by using the satellite's orientation parameters and a small number of ground control points (GCP). While Digital Globe provides users with the full photogrammetric model of QuickBird, Space Imaging does not disclose the physical camera model or the ephemeris data of Ikonos but instead provides rational polynomial coefficients (RPCs) to describe the mathematical relationship between object and image coordinates (Grodecki 2001). This has brought about the development and evaluation of RPC-based methods for orthorectification and spatial intersection for both Ikonos and QuickBird images. Dial *et al.* (2003) showed that the discrepancy between the RPC and physical camera

models does not exceed 0.04 pixels in the case of Ikonos images. Using RPCs, a few ground control points and a precise DSM, Ikonos images could be orthorectified with errors of 1 m or less (Fraser *et al.* 2002, Helder *et al.* 2003, Toutin 2003, Eisenbeiss *et al.* 2004, Poon *et al.* 2005). Similar results were obtained with QuickBird images (Noguchi *et al.* 2004, Toutin 2004). Precise DSMs were generated using RPC-based bundle adjustment and stereo-matching techniques adapted to the Ikonos or QuickBird sensor characteristics. Elevation root mean square errors (RMSE) of 0.9 m or less on independent ground control points have been reported (Fraser *et al.* 2002, Zhang *et al.* 2002, Poon *et al.* 2005). Image-matching uncertainty over complex surfaces such as forest canopies and urban areas led to a lower vertical accuracy, as studies comparing stereo-Ikonos and lidar DSMs revealed (Eisenbeiss *et al.* 2004, Toutin 2004, Poon *et al.* 2005). For example, Poon *et al.* (2005) found an average 2.7 m RMS elevation difference between an Ikonos and a lidar DSM used as reference, but observed discrepancies of 5.3 m in forested areas.

We hypothesize that measurements of the elevation differences between DSMs created from stereo satellite images and highly accurate lidar DTMs could generate a hybrid CHM with good height accuracy over relatively large areas. There is a good potential for applying this method as the accumulated, archived lidar DTM data are covering more and more forest land. It could for example reach at least 1 000 000 km^2 by 2010 in the USA alone (Stoker *et al.* 2006). This estimate does not include the numerous private non-inventoried surveys. Certain European countries are also partly or entirely covered. Because ground elevations are quite stable in time over most areas, new maps of height or biomass could be produced simply by processing stereo satellite images and transforming the resulting DSM into a CHM using the lidar ground elevations. The images themselves can also be used to obtain information on other attributes such as species and health. Once such CHMs are calibrated over different forest types, recalibration for other scenes should not be necessary because radiometric variations caused by atmospheric or topographic conditions essentially do not affect the reconstruction of height from stereo-matching.

The general objective of this study is to assess the accuracy of canopy height and above-ground biomass estimates extracted from a CHM generated by combining a DSM derived from a stereo-pair of Ikonos images and a lidar DTM. We proceed by first verifying the accuracy of the height information using field measurements of individual trees and the all-lidar CHM used as a reference. We then assess the error of Ikonos-lidar average height and above-ground biomass estimates by comparing these with field data on a plotwise basis. Throughout our study, commercial off-the-shelf products were used, reflecting our intention to propose an approach that is of practical relevance and that can be readily implemented or replicated.

2. Study area and datasets

The study site consists of a 110 km^2 area corresponding approximately to the territory of the Training and Research Forest of Lake Duparquet (TRFLD), located in Quebec, Canada (79°22′ W, 48°30′ N). The rolling hill topography with elevations between 227 and 348 m above sea level is essentially covered by lacustrine clay deposits and shallow tills (Brais and Camiré 1992). The forest vegetation is typical of the south-east boreal forest, characterized by an abundance of stands of mixed composition. Balsam fir (*Abies balsamea* L. [Mill.]) is the dominant species in mature forests. It is associated with white spruce (*Picea glauca* [Moench] Voss), black spruce

(*Picea mariana* [Mill] B.S.P.), white birch (*Betula paprifera* [Marsh.]), trembling aspen (*Populus tremuloides* [Michx]), and jack pine (*Pinus banksiana* Lamb.). Various other species are also found. Approximately one fourth of the area is under conservation and bears older forests influenced by gap dynamics. The remaining of the study area is managed and contains clear cuts, partial cuts, as well as regeneration zones and mature stands. The overall age structure found at this site results mostly from a fire-driven disturbance regime and recent but limited harvesting activities.

The dataset used in this study is composed of a lidar coverage, a stereo-pair of IKONOS images, aerial photographs, and field data. The lidar survey was carried out from 14 to 16 August 2003 using Optech's ALTM2050 instrument flown at 1000 m above-ground level with a maximum scan angle of 15° and a 50% overlap between adjacent strips. First and last returns were recorded for each pulse at a pulse repetition rate of 50 000 Hz. The data were registered to high-end carrier phase differential GPS ground profiles, and the inter-strip geometrical fit was improved using the TerraMatch™ algorithm by Terrasolid Ltd (Helsinki). The last returns were classified by the survey provider as being ground or non-ground using Terrasolid's Terrascan™, followed by manual verification and editing. Average densities of first and ground-classified last returns were respectively 3.0 and 0.2 hit(s)/m^2.

One Ikonos stereo pair (figure 1) was captured in-track on 5 September 2003 (3 weeks after the lidar dataset) in full leaf-on conditions and was purchased as an epipolar-resampled Ikonos reference level product. The 11-bit panchromatic images forming the stereo pair had a nominal ground pixel size of 1 m and determined a base-to-height ratio of 0.8. Each had a field of vision of approximately 10.3 by 10.7 km. The resulting stereo-overlap area slightly exceeded 100 km^2. The RPCs supplied with the images had a nominal planimetric accuracy of 25 m CE90 and a vertical accuracy of 22 m LE90 (exclusive of relief displacement). The elevation and azimuth angles of both sun and sensor at the time of image acquisition are given in table 1. The images were very clear, with the exception of two very small clouds and corresponding shadows (bottom right corner of images in figure 1). Black and white metric photographs at a scale of 1 : 15 000 were acquired in May 2003. They were used to locate individual trees to be measured in the field and to compare satellite-based to aerial-based height measurements.

Field data were collected for the verification of individual tree heights, plotwise average height of dominant trees, and above-ground biomass (hereafter termed 'biomass' for brevity). The height of 211 individual trees was measured *in situ* during the summer of 2003 using a Vertex III clinometer's (Haglöf, Sweden). Printouts of 1 : 15 000 aerial photographs acquired in 2003 were carried in the field to mark the position of all the measured individual trees. In addition, a total of 43 plots each measuring 20 × 20 m were inventoried in 2003 and 2005 to gather reference data on average height. For each plot, the heights of three dominant trees were measured and averaged. The 2005 heights were not corrected for growth because the measured trees were located on poor sites or were over-mature for the most, thus experiencing very limited growth. To acquire data on biomass, the diameter at breast height (DBH) and species were recorded for all trees above a threshold DBH measured in 57 plots of 400 m^2 between 2002 and 2005. Many of the above-mentioned 2003 height plots were also biomass plots. The threshold DBH varied between plots depending on the average tree size, up to a maximum value of 9 cm. The DBH and species data were used to predict biomass on an individual tree basis using the general deciduous and coniferous equations published in Lambert *et al.* (2005).

Table 1. Sun and sensor elevation and azimuth angles (°).

	Sun		Sensor	
	Elevation	Azimuth	Elevation	Azimuth
Image A	47.28	162.50	67.48	27.83
Image B	47.33	162.93	67.43	180.52

Total above-ground biomass per plot was calculated by summing the predicted individual values. All plot positioning was done using a Panasonic SXBlue real-time differential GPS (Geneq, Montreal) allowing an accuracy of 2–3 m under canopy. The general statistics of the measured trees and plots are presented in table 2.

3. Methods

3.1 *Preparation of the lidar models*

Raster lidar models were prepared for a number of purposes in the study. The lidar DSM was used as a surrogate source of ground control point data, the lidar CHM served as a reference for canopy height in one stage of the validation, and the lidar

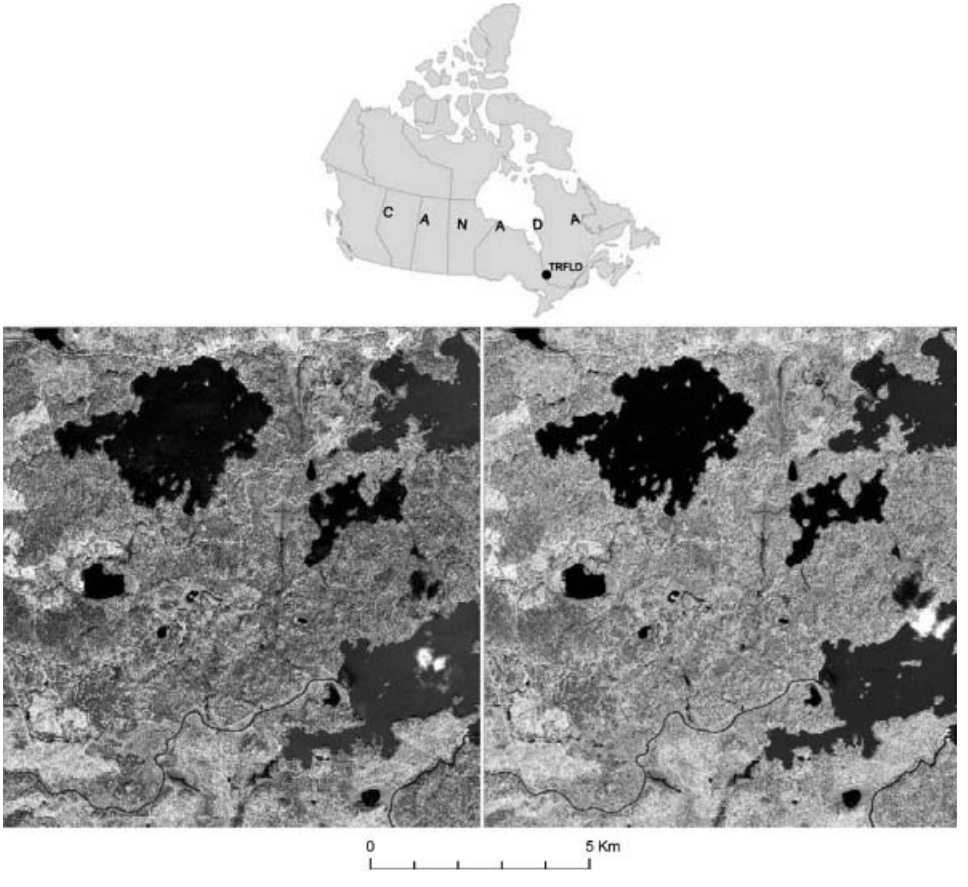

Figure 1. Ikonos stereo pair. Images measure 10.3 × 10.7 km.

Table 2. Field data summary statistics.

	n	Min	Max	Mean	SD
Individual trees (height in m)	211	7.1	33.1	23.9	4.9
Height plots (average dominant height in m)	43	4.5	32.6	21.5	7.2
Biomass plots (above ground biomass in $Mg\,ha^{-1}$)	57	6.2	606.7	152.5	101.0

DTM was required to compute the all-lidar and the Ikonos-lidar CHMs. The DSM was created by interpolating all first returns using the IDW (Inverse Distance Weighing) method implemented in ArcGIS v. 9.1 (ESRI). To remove inner-crown hits, a modified median filter was applied to the interpolated grid. The height value of the centre cell of a 3×3 filter was replaced by the window's median value if it was at least 0.25 m lower than the window's median. This threshold and the filter size were chosen empirically with the goal of filling small inner-crown holes while preserving larger inter-tree gaps. The lidar DTM was created by interpolating the ground-classified last returns. DTM pixels were given the value of the lowest lidar return value falling therein. Empty pixels were filled by interpolating the surrounding values using the IDW method. Finally, the lidar CHM was computed by subtracting the lidar DTM from the filtered lidar DSM. All lidar models were generated at a 1 m ground pixel size.

3.2 *Registration of the Ikonos stereo-pair*

Overlaying the original Ikonos images on to the lidar models revealed a horizontal bias of at least 10 m in flat areas. Because ground control points are difficult to acquire in this remote area as there are very few buildings or man-made structures that could be used for such purpose, and because the following analyses required that the Ikonos stereo-pair be registered relatively to the lidar models, we developed a new automated shadow-based co-registration method using the lidar DSM at the 3D geoposition reference. Shadows were cast on surfaces according to the lidar DSM geometry and based on the Sun's position at the precise image-acquisition time recorded in the metadata of the Ikonos images. The shadows visible from the satellite platform were then projected onto the Ikonos images using the original RPC and offset values. For a given image, the X and Y offset values (*LineOffset* and *SampOffset* Ikonos parameters) were incremented iteratively within a 2D search space defined by the maximum expected planimetric shift. The cast shadows where reprojected on the image plane for each increment, and the average image brightness within projected shadows was computed. As shadows are generally the darkest objects within an image, the XY offsets that yielded the lowest average brightness in shadows were assumed to be the correct geoposition values. This procedure was performed independently for each image. Sub-images were used to accelerate computations. We then calculated the shift in pixels and lines necessary to align the Ikonos images with the lidar DSM (i.e. the difference between the initial and corrected offset values). Note that the underestimation of tree height caused by the absence of a lidar return on the tree tip on a certain proportion of trees leads to a shortening at both extremities of a lidar-predicted tree shadow, i.e. at its origin near the crown centre, and at the farthest point of its projection. Therefore, the underestimation of tree height is not theoretically expected to cause a bias in the XY registration procedure. Verification GCPs were then acquired on both images to assess the accuracy of the shadow-based method. An interpreter linked the lidar

XYZ values of characteristic points of the virtual lidar shadow image to the corresponding Ikonos conjugate points. Twenty-five points consisting of the tip of conifer tree shadows cast on roads were collected on both images. The *XYZ* position was calculated from the conjugate points using an RPC-based spatial intersection method summarized in the subsequent lines. For each pair of conjugate points in the stereo images, the approximate *X*, *Y*, and *Z* coordinates of the corresponding treetop were obtained by solving the rational functions with only their constant and first-order terms. Then, the approximate coordinates were corrected iteratively by a least-squares adjustment using all the terms of the third-order rational functions. The correction was stopped if the residuals at *X*, *Y*, and *Z* were smaller than 0.1 m. This method is described in greater detail in Hu *et al.* (2004). The overall RMSE of the 25 verification GCPs was calculated by first computing their *XYZ* positions based on the original and corrected offset values respectively. These positions were then compared with the corresponding lidar DSM positions. Because the verification GCPs corresponded only to the tip of shadows which represent a very small fraction of all the shadow pixels used in the registration procedure, they provide an essentially independent check of the registration accuracy. However, lidar underestimation of tree height might introduce a small bias in the verification GCPs coordinates. The degree of underestimation and bias should likely remain very small because of the high return density (3.0 returns/m^2).

3.3 *Assessing the accuracy of height information on an individual tree basis*

The first stage of the Ikonos-lidar height information quality assessment consisted in quantifying the error of manual measurements of individual tree height. This approach was used to isolate the photogrammetric error attributable to the joint geometry of the combined dataset (DTM accuracy, co-registration quality and photogrammetric exactness) from other sources of uncertainty. This is justified by the fact that later tests on the quality of plotwise mean height of the Ikonos-lidar CHM characterize the compound error resulting jointly from the photogrammetric uncertainty, the plotwise height averaging process, and the stereo-matching problems. We measured the image coordinates of the conjugate points corresponding to 112 individual treetops ranging from approximately 7 m to 33 m (comprising deciduous and coniferous species) from the 211 tree heights that were measured on the ground. Only trees that could be unambiguously identified on both Ikonos images and linked to *in situ* measurements were kept. The interpreter was trained at identifying treetop conjugate points by trying to perform measurements that corresponded with the field data using 13 training trees. Afterwards, he measured the remaining 99 trees without knowledge of the field height. The treetop elevations were then computed using the RPC-based 3D intersection method. Tree heights were obtained by subtracting the underlying ground heights read from the lidar DTM at the *XY* position of the treetop. For comparison purposes, the heights were also extracted using respectively the photo-lidar approach and the all-lidar CHM. The former method uses a combination of an aerial photograph stereo-model and a lidar DTM in the same way as in the Ikonos-lidar approach. The stereo-model registration and the manual photo-lidar heights measurements were performed using the method described in St-Onge *et al.* (2004) on the 2003 stereo-pairs. Tree heights were also estimated using the all-lidar CHM by manually extracting the highest height value within individual crowns. The respective accuracy of the Ikonos-lidar, photo-lidar and all-lidar height values was assessed by comparing

them with the *in situ* measurements. This comparison involved the calculation of the bias and regressions between remote sensing and field values.

3.4 *Assessing the accuracy of the Ikonos DSM and the Ikonos-lidar CHM*

To generate an Ikonos-lidar CHM, we first created an optimal DSM from the corrected Ikonos stereo-pair using PCI's OrthoEngine™ (v. 10) image-matching function. We produced 20 DSMs using different combinations of matching window size, resolution, and hole-filling options. A visual comparison with the lidar DSM showed that the DSM created at a 2 m resolution with the hole-filling option had the highest quality. This Ikonos DSM was then resampled at a 1 m resolution to match that of the lidar DSM. Featureless areas, such as lakes, rivers, and clouds, were masked out because they lack image details required for image matching. Cloud shadows were also removed. To create the mask, a 1 : 20 000 vector map of the water bodies with an added 20 m buffer was first rasterized. We then manually generated an additional raster mask for the clouds and the cloud-shadowed areas. The masks were applied to the optimal photogrammetric DSM. To evaluate the overall accuracy of that DSM, we compared the lidar and Ikonos DSMs by computing the inter-DSM difference (lidar minus Ikonos, i.e. the overall bias of the Ikonos DSM) and the RMSE. Using thresholds on the lidar CHM, these inter-DSM metrics were also calculated separately for the three strata bare ground, regeneration, and forested areas, classified respectively by applying the lidar CHM height thresholds <0.5 m, 0.5–5 m, and >5 m.

The 1-m-resolution Ikonos-lidar CHM was created by subtracting the lidar DTM from the optimal masked Ikonos DSM. The mean Ikonos-lidar CHM height and the heights at the 0th, 50th, 75th, 90th, 95th, 99th, and 100th percentiles were extracted from both the Ikonos-lidar and all-lidar CHMs. Extractions were performed on 400 m^2 windows that corresponded exactly to the 43 field plots. Emphasis was put on the higher percentiles, as these often correlate more to forest height than lower ones. A linear regression between, on the one hand, the Ikonos-lidar as well as the all-lidar CHM metrics and, on the other hand, the mean plotwise field heights was performed. In order to widen the comparison between the two types of CHMs, the height metrics were also extracted from arbitrary 20 m $\times$ 20 m plots (without field reference), spaced 100 m in both X and Y directions and spread over the entire stereo-overlap area. This resulted in a total of 4803 'virtual' plots. Linear regressions were computed between every possible combination of Ikonos-lidar and all-lidar CHM metric (e.g. Ikonos-lidar at 90th percentile with all-lidar at 95th percentile, etc.), using the lidar values as the independent variable. The 100 m spacing was chosen to minimize the effect of spatial auto-correlation on the regression results.

Finally, the accuracy of Ikonos-lidar biomass estimates was evaluated. As a preliminary analysis, the statistical relationship between the *in situ* average dominant height and the biomass was determined through regression for the height plots only. This was done for the purpose of evaluating the true strength of the height–biomass relationship. Then, the Ikonos-lidar and all-lidar CHM height metrics were extracted and used to predict biomass for all 57 biomass plots. Initial tests showed that the relationships between the *in situ* biomass values and the CHM metrics were nonlinear. Linear regressions were therefore performed on log-transformed values, and regression statistics are reported.

4. Results

The planimetric shifts between the original and corrected offset values amounted to −10.784 lines and −11.696 columns in one image, and −9.748 lines and −12.226 columns in the other. The positioning accuracy computed for the original and corrected offset values using the 25 lidar verification GCPs is presented in table 3. After correction, the average positional bias dropped to near zero values. The remaining RMSE was below 1 m in X, Y, and Z.

Individual tree heights were measured manually on the coupled Ikonos-lidar models with a mean error (bias) of −2.58 m (table 4), which is significantly more than what was achieved using the aerial photo-lidar dataset (−0.57 m). The initial lidar statistics were strongly influenced by a single but far outlier, apparently caused by a tall conifer tree that was almost entirely missed by lidar hits. This outlier was removed because of its disproportionate influence on the statistics and the regression line. As a consequence, the lidar bias dropped from −2.03 m to −1.84 m. The manual Ikonos-lidar measurements were highly correlated to field heights, with a coefficient of determination of 0.87, which is clearly lower than that of the photo-lidar heights (0.95) but still higher than that of lidar (0.84 after outlier removal). The standard error of the estimate of the regression involving Ikonos-lidar measurements was quite low at 1.66 m and remained between that of the photo-lidar (1.11 m) and the all-lidar (2.07 m) values.

The Ikonos-lidar CHM produced with the optimal photogrammetric DSM is shown in figure 2, with the corresponding lidar CHM and difference image. Overall, canopy height patterns are very similar, but the lidar CHM has a better resolution than the Ikonos-lidar CHM. This is apparent in the sub-image presented at a much larger scale in figure 3. The detail of individual trees visible in the all-lidar CHM is lost in the Ikonos-lidar version, but fine-scale patterns are still easily perceivable in the latter.

The quantitative differences between the lidar and Ikonos DSMs are reported in table 5. As expected, the Ikonos DSM surface is very close to the lidar one in bare areas, but greater differences exist for vegetated areas, especially for taller forests. The overall bias of the Ikonos DSM is below 1 m in all cases and surprisingly low for forested areas (−0.38 m). However, the RMSE results clearly show that stereo-matching yields more accurate results over bare areas than over developed forests.

The mean height and the height at percentiles 0, 50, 75, 90, 95, 99, and 100 were predicted for the 43 field plots based on the Ikonos-lidar and the all-lidar CHMs, respectively. The coefficients of determination (R^2) of the regression between the average dominant heights measured in the field as well as the CHM metrics are presented in table 6. Plotting the data revealed that most Ikonos-lidar height estimates were close to the regression line, with the notable exception of five clear outliers that obviously resulted from local stereo-matching blunders. When these

Table 3. Positioning accuracy resulting from the original and corrected Ikonos offset values (metres).

	Original offsets			Refined offsets		
	X	Y	Z	X	Y	Z
Mean	−11.79	10.39	−1.26	0.02	−0.05	0.07
RMSE	11.81	10.43	1.30	0.57	0.60	0.36

Table 4. Individual tree height measurement error.

	Ikonos-lidar	Photo-lidar	Lidar (all trees)	Lidar (minus 1 outlier)
Mean difference (m)	−2.6	−0.6	−2.0	−1.8
SEE (m)	1.7	1.1	2.6	2.1
R^2	0.87	0.95	0.75	0.84

outliers were removed (leaving 38 plots), the maximum Ikonos-lidar R^2 increased from 0.53 to 0.91, approaching the lidar maximum of 0.95. The standard error of the estimate resulting from the best Ikonos-lidar regression equation (i.e. for the 100th percentile height, after outlier removal) was 2.08 m. The highest proportions of explained variance were observed at the higher percentiles, for both the Ikonos-lidar and all-lidar CHMs.

The coefficients of determination of the regressions between the Ikonos-lidar and the all-lidar CHM metrics extracted from the 4803 virtual plots are reported in table 7. For brevity, we present only the homogeneous metric combinations (e.g. lidar 90th percentile with Ikonos-lidar at the 90th percentile), as their relationship was always stronger than that of the corresponding heterogeneous pairs. The highest prediction power was observed for the mean and for the height at the 50th and 75th percentiles. The standard error of the estimate resulting from the best regression (mean height with an R^2 of 0.87) was 1.90 m.

Before assessing the accuracy of the Ikonos-lidar biomass prediction, the average dominant heights calculated from field measurements in 43 plots were regressed against the corresponding *in situ* biomass values. An R^2 of 0.79 was obtained for the log-transformed variables. No saturation was found, as height continued to increase with biomass, even at biomass values exceeding 500 Mg ha^{-1} (figure 4). This indicates that estimating biomass based on canopy height might overcome the common saturation problem encountered when using image brightness.

Table 8 shows the coefficient of determination of the regressions between the field biomass and the metrics extracted from the Ikonos-lidar and all-lidar CHMs (after log transformation). Plotting the data revealed the presence of two clear outliers. These data points were also located away from the main point cloud in the lidar plot. They were removed from both the Ikonos-lidar and the all-lidar datasets, leaving 55 plots. The best relationship between *in situ* biomass and the Ikonos-lidar metrics was for the height at the 99th percentile (R^2 of 0.79, after outlier removal). For lidar, the height at the 75th percentile provided the best prediction, with an R^2 of 0.87. The corresponding RMSEs for the Ikonos-lidar and lidar metrics were respectively 70.57 and 62.55 Mg ha^{-1}. The estimate for one plot with an exceptionally high value of 606 Mg ha^{-1} was largely underestimated by both types of CHMs. If this additional plot is removed, the RMSE drops to 50 and 41 Mg ha^{-1}, respectively, for the Ikonos-lidar and lidar CHMs. Overall, the very high values of biomass were poorly predicted by both the Ikonos-lidar and the lidar CHM. Figures 5 and 6, showing predicted against actual values, reveal that biomass appears to saturate with CHM height at around 300 Mg ha^{-1} for both types of CHMs. Because lidar height at the 75th percentile may not reflect the height of the tallest trees (a fact that would potentially limit the predictive capacity of lidar for high biomass plots), an alternative model using maximum lidar height was computed. However, this model did not improve the capability of predicting very high biomass values.

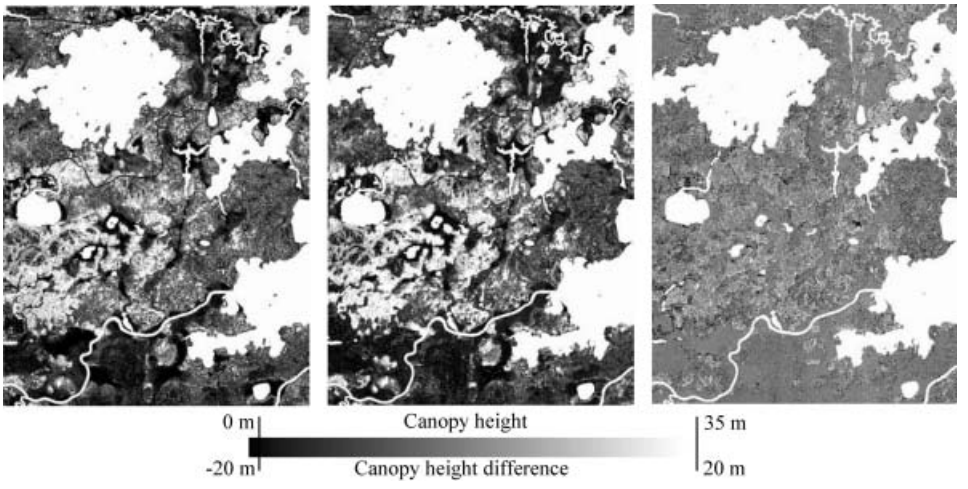

Figure 2. From left to right: the all-lidar CHM, the Ikonos-lidar CHM, and the difference image. The displayed sector measures 7.8 km × 10.3 km. Brightness is proportional to canopy height or height difference. Plain white areas correspond to the mask.

5. Discussion

Co-registration and individual tree height results are consistent with previous studies that demonstrated the photogrammetric quality of Ikonos imagery (Fraser *et al.* 2002, Helder *et al.* 2003, Toutin 2003, Eisenbeiss *et al.* 2004, Poon *et al.* 2005). The RMSE of the test control points are, for example, similar to the values reported by Fraser *et al.* (2002), and indicate that co-registration should not create a significant bias in the height measurements. The downward bias of 2.58 m of Ikonos-lidar manual tree height measurements is most likely due to the level of resolution. It is a well-known fact that the amount of downward bias in stereo-photogrammetric measurements of tree height is inversely proportional to resolution. Spurr (1960, p. 363) suggested various corrections in tree height according to photographic scale, reaching 1 m (3 feet) for 'normal crowns' at 1 : 20 000. Given that Ikonos images

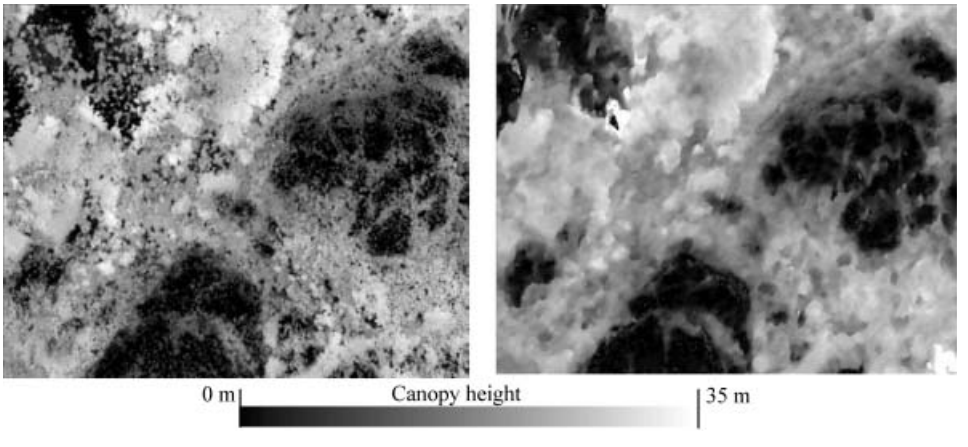

Figure 3. Zoomed windows of the all-lidar CHM (left) and corresponding Ikonos-lidar CHM. Windows are 750 m wide.

Table 5. Statistics of differences between the lidar and Ikonos DSMs by cover type (m).

	Bare	Regeneration	Forested
Mean difference (bias)	0.74	0.93	−0.38
RMSE	1.23	2.62	4.24

clearly have a lower resolution than 1 : 20 000 photographs, the bias of −2.58 m appears consistent with expectations derived from this scale–bias relationship. It is interesting to note that the bias observed for the photo-lidar measurements in this study (−0.58 m) is very close to the value proposed for normal crowns by Spurr (1960) at the same photographic scale of 1 : 15 000, i.e. −0.61 m (−2 feet). The low residual error of individual tree height measurements after correction by a regression equation (SEE of 1.66 m) also demonstrates that the joint Ikonos-lidar geometry is of a very high quality. This residual error may be attributable to a minor photogrammetric uncertainty, slight interpretation errors in pinpointing treetops, and field measurements, in particular for tall deciduous trees. Moreover, the fact that the lidar RMSE was larger than that of the Ikonos or photo-lidar measurements is probably due to laser pulses missing the apex of conifer trees. Because of their elongated shape, the vertical error increases rapidly with the planimetric distance between the apex and the closest lidar return. As this distance varies significantly from tree to tree, the height error fluctuates by a considerable amount, resulting in a relatively large RMSE.

The findings concerning the geometric quality of the coupled Ikonos-lidar models strongly suggest that errors in the Ikonos DSM and the Ikonos-lidar CHM are essentially caused by image-matching errors and artefacts. The quality of the Ikonos DSM appeared similar to what was reported in previous studies (Eisenbeiss *et al.* 2004, Poon *et al.* 2005). Errors increased as the surface becomes more complex, being maximum over mature forest canopies. The RMSE value of 4.24 m is similar to values of 5.3 m reported by Poon *et al.* (2005) for forest covers. The very low bias over forest canopies (−0.38 m) is likely due to chance cancellations between under- and overestimations. Lidar reconstructs the peaks and troughs of the canopy quite accurately, while the image-matching process tends to smoothen out asperities and fill gaps to some extent.

As this is the first time that canopy height is mapped using a combination of high-resolution stereo space imagery and lidar, results cannot be directly compared with that of previous studies. In general, however, findings are consistent with those obtained by combining stereo-aerial imagery and lidar (St-Onge *et al.* 2006), or stereo-aerial imagery and other types of DTM data (Miller *et al.* 2000, Zagalikis *et al.* 2005) in that the general height patterns are well reconstructed (as evidenced by the high correlation between Ikonos-lidar and lidar metrics in the 4803 virtual plots) and in that fine details such as individual crowns or small gaps are not resolved.

Table 6. Coefficients of determination (R^2) of Ikonos-lidar and all-lidar CHM metrics for plotwise average dominant height.

	Mean	0th	50th	75th	90th	95th	99th	100th
Ikonos-lidar	0.42	0.29	0.39	0.48	0.50	0.52	0.52	0.53
Ikonos-lidar minus 5 outliers	0.72	0.45	0.68	0.82	0.85	0.88	0.90	0.91
All-lidar minus 5 outliers	0.86	0.21	0.89	0.93	0.94	0.94	0.95	0.93

Table 7. Coefficients of determination (R^2) between all-lidar and Ikonos-lidar metrics for virtual plots.

Mean	0th	50th	75th	90th	95th	99th	100th
0.87	0.38	0.85	0.85	0.83	0.79	0.72	0.66

Despite this limitation, small tree groups and larger gaps were well recognizable on the Ikonos-lidar CHM. Matching blunders due to left–right image dissimilarities caused by the roughness of the canopy surface also occurred locally. At the scale of plots, the results were less accurate than lidar, although not considerably less. Metrics extracted from the Ikonos-lidar height distribution within a plot are on average quite similar to their lidar equivalent, contrary to spot heights (at pixel level) that may sometimes be very different.

The biomass estimates extracted from the all-lidar CHM have accuracies similar to those reported in several previous studies that used lidar height percentiles as predictors. We found an RMSE of 41 $Mg\,ha^{-1}$ (after outlier removal), while other studies report RMSEs between 29 and 50 $Mg\,ha^{-1}$ for above ground biomass values not exceeding approximately 320 $Mg\,ha^{-1}$ (Lim *et al.* 2003, Lim and Treitz 2004, Patenaude *et al.* 2004). However, the characteristics of the forest we studied are somewhat different from those analyzed in previous work. In many regards, canopies of the study area are complex, with mostly mixed stands, age variations from a few years to a few centuries, managed and natural stands as well as a very wide range of biomass per hectare, comprising locations where it exceeds 600 $Mg\,ha^{-1}$. Moreover, the Ikonos-lidar biomass predictions were slightly less accurate than the corresponding lidar estimates. The only somewhat comparable study (Zagalikis *et al.* 2005) reported relative biomass errors between −4.7% and

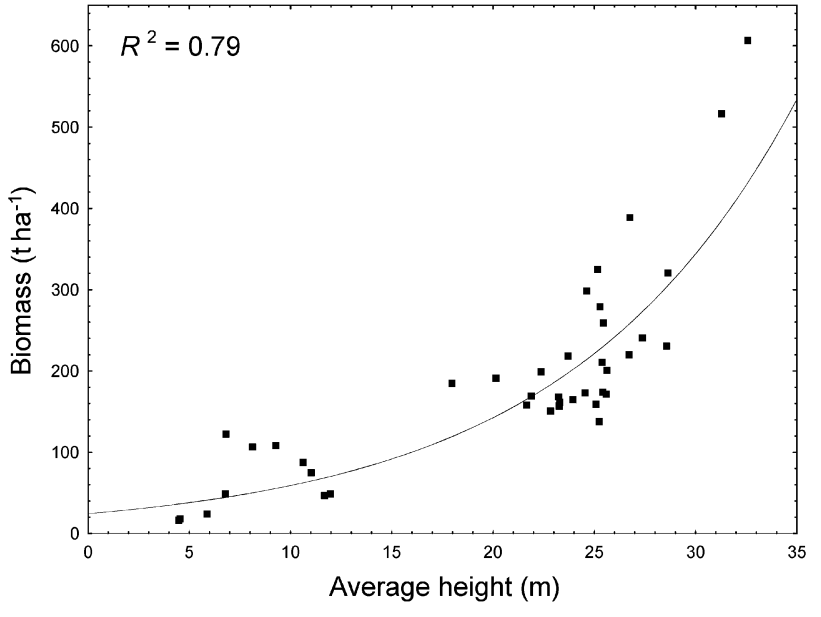

Figure 4. Relationship between average dominant plot height and above-ground biomass based on *in situ* values.

Table 8. Coefficients of determination for biomass prediction equations for Ikonos-lidar and all-lidar CHMs (after log–log transformation).

	Mean	0th	50th	75th	90th	95th	99th	100th
Ikonos-lidar	0.67	0.50	0.65	0.66	0.69	0.70	0.71	0.70
Ikonos-lidar (minus 2 outliers)	0.76	0.50	0.75	0.76	0.78	0.78	0.79	0.78
All-lidar	0.81	0.54	0.71	0.83	0.82	0.81	0.79	0.74
All-lidar (minus 2 outliers)	0.86	0.54	0.82	0.87	0.85	0.85	0.83	0.78

−61.8% which cannot be compared directly to our absolute RMSE values. Contrary to several results obtained using multispectral or radar images, saturation at relatively low biomass values (circa 150–200 Mg ha^{-1}) did not occur. It did, however, appear at much larger values (around 300 Mg ha^{-1}) in both the lidar and Ikonos-lidar datasets. As only a very small number of plots exceeded 300 Mg ha^{-1}, it is premature to conclude that CHMs cannot reflect very large biomass values. Trees in the highest biomass plots were indeed slightly higher (by 2–3 m) than those in plots having 300–400 Mg ha^{-1}. This small height difference was detected by neither the Ikonos-lidar nor the lidar CHM.

To apply the Ikonos-lidar method in an operational manner, precise field data should be collected to calibrate regression models for predicting average dominant tree height and biomass on a plotwise basis. An independent set of field plots should also be used to assess the accuracy of the prediction. We surmise that within an ecoregion presenting somewhat homogeneous forest conditions making for relatively stable allometric relationships between height and biomass, a single calibration should suffice to apply the Ikonos-lidar approach to different scenes across space and time. In principle, the estimation of average tree height should not be affected by moderate variations in Sun elevation, topography, reflectance of the

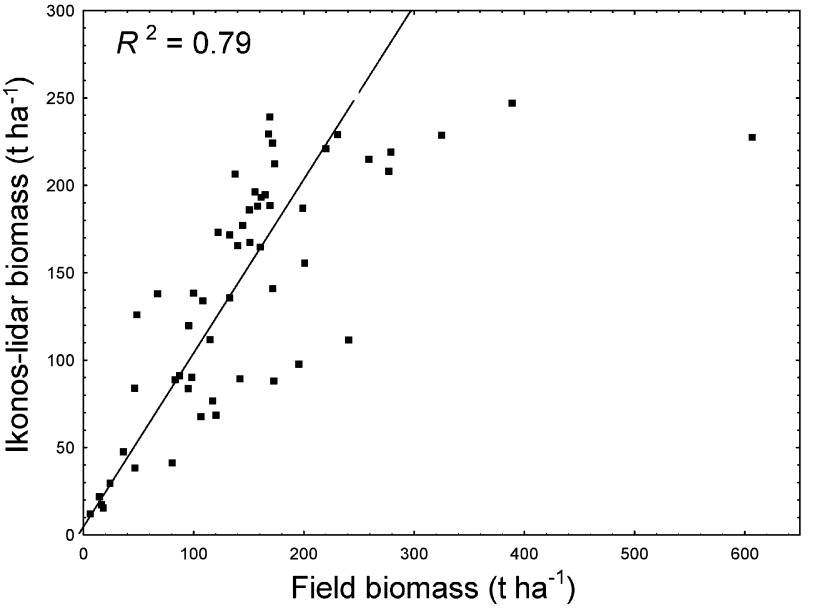

Figure 5. Relationship between field biomass and values predicted using the Ikonos-lidar CHM (with 1 : 1 line).

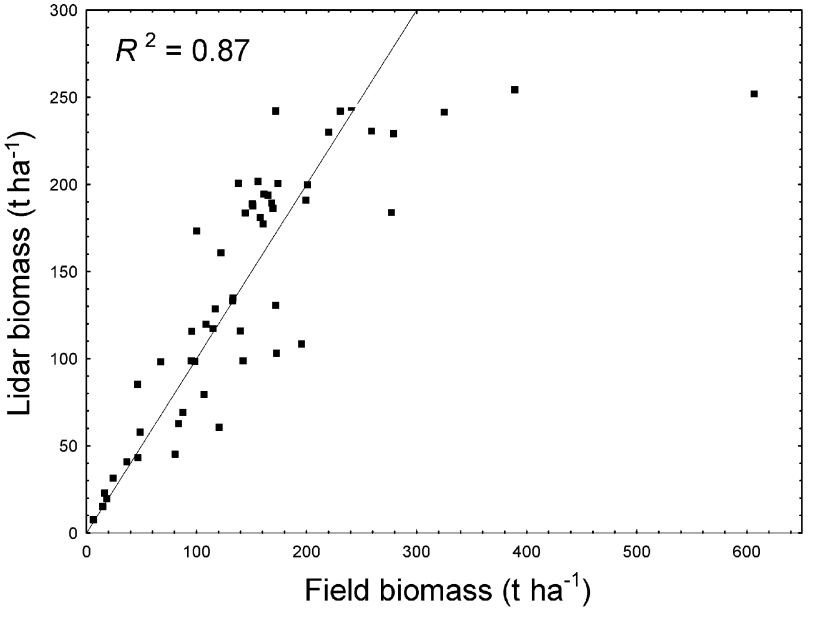

Figure 6. Relationship between field biomass and values predicted using the all-lidar CHM (with 1 : 1 line).

vegetation and other factors influencing brightness because these factors do not affect the stereo-matching results significantly. This would therefore represent a more robust remote sensing approach to biomass quantification and mapping. Given that lidar DTM data exist for an area, purchasing and processing a single Ikonos stereo-pair is rather inexpensive and straightforward, and provides relatively accurate estimates of biomass over more than 100 km^2. Because lidar coverages are rapidly increasing, the applicability of the Ikonos-lidar approach will rapidly improve.

This study likely provides a lower bound for the accuracy of biomass assessment using lidar and Ikonos images. Improvements in the accuracy of stereo matching should help produce more accurate DSMs, approaching the quality of lidar ones. For example, the EHTZ image-matching method recently proposed by Baltsavias *et al.* (2006) produced a DSM from stereo Ikonos images that constituted a clear improvement over the corresponding DSM generated by a commercial package (SOCET SET). It showed a very high resolution, with some individual trees being resolved in 3D and the canopy surface reconstructed even in cloud shadows. These improvements would propagate to the Ikonos-lidar CHM, leading to more accurate height and biomass predictions.

6. Conclusions

This study demonstrated the possibility of measuring individual tree height manually and of mapping canopy height and biomass automatically by using a combination of stereo Ikonos images and a lidar DTM. Error analyses showed that the overall photogrammetric quality of the co-registered Ikonos and lidar models is very high. Consequently, the unexplained variance in average height and biomass estimates can be attributed mostly to image matching inaccuracies and other factors.

We also found that height percentiles extracted plotwise from an Ikonos-lidar CHM had a predictive power for average height and biomass that approaches that of the corresponding all-lidar CHM. This implies that, because remotely sensed height percentiles do not suffice to explain all the variance in biomass, image matching problems are not the sole cause of uncertainty in predicting biomass based on an Ikonos-lidar combination. Moreover, we did not observe saturation of CHM metrics (either lidar or Ikonos-lidar ones) with increasing biomass in the range 0–300 $Mg\,ha^{-1}$ (a threshold that is much higher than those reported in studies using image brightness). This apparent saturation existed despite the fact that, according to field data, average plot height and biomass continue to covary at extreme levels (even above 500 $Mg\,ha^{-1}$). However, the data used in this study were not sufficient to conclude that saturation does indeed occur at high levels (above 300 $Mg\,ha^{-1}$) because very few plots reached such biomass values.

The Ikonos-lidar approach represents a practical solution for rapidly updating forest height and biomass information over relatively large areas with a fair accuracy, for zones where lidar DTMs exist. It can represent a practical and economical alternative to the repeated acquisition of lidar data from an aerial platform. Given that *in situ* calibration data should not be required for every new stereo-pair, the Ikonos-lidar method should be reproducible throughout scenes without re-calibration. Finally, improvements in image-matching methods can be expected to increase the accuracy of Ikonos-lidar CHMs and improve the height and biomass estimates.

Acknowledgements

The authors wish to acknowledge the financial help of the BIOCAP Foundation of Canada, of the Canadian Foundation for Innovation, and of the Natural Sciences and Engineering Council of Canada. We also thank the three anonymous reviewers for their valuable suggestions.

References

ANDERSEN, H.-E., MCGAUGHEY, R.J., CARSON, W.W., REUTEBUCH, S.E., MERCER, B. and ALLAN, J., 2003, A comparison of forest canopy models derived from lidar and InSAR data in a Pacific Northwest conifer forest. In *ISPRS Workshop on 3-D Reconstruction from Airborne Laser Scanner and InSAR Data*, October 2003, Dresden, Germany, pp. 211–217.

AUSTIN, J.M., MACKEY, B.G. and VAN NIEL, K.P., 2003, Estimating forest biomass using satellite radar: an exploratory study in a temperate Australian Eucalyptus forest. *Forest Ecology and Management*, **176**, pp. 575–588.

BALTSAVIAS, E., GRUEN, A., KÜCHLER, M., THEE, P., WASER, L.T. and ZHANG, L., 2006, Tree height measurements and tree growth estimation in a mire environment using digital surface models. In *Workshop on 3D Remote Sensing in Forestry*, 14–15 February, Vienna, 2006.

BALTZER, H., 2001, Forest mapping and monitoring with interferometric synthetic aperture radar (InSAR). *Progress in Physical Geography*, **25**, pp. 159–177.

BRAIS, S. and CAMIRÉ, C., 1992, Keys to soil moisture regime evaluation for northwestern Quebec. *Canadian Journal of Forest Research*, **22**, pp. 718–724.

DIAL, G., BOWEN, H., GERLACH, F., GRODECKI, J. and OLESZCZUK, R., 2003, IKONOS satellite, imagery, and products. *Remote Sensing of Environment*, **88**, pp. 23–36.

EISENBEISS, H., BALTSAVIAS, E., PATERAKI, M. and ZHANG, L., 2004, Potential of IKONOS and QuickBird imagery for accurate 3D point positioning, orthoimage and DSM

generation. *International Archives of the Photogrammetry, Remote Sensing and Spatial Information Sciences*, **35**, pp. 522–528.

FANG, J., BROWN, S., TANG, Y., NABUURS, G.-J., WANG, X. and SHEN, H., 2006, Overestimated biomass carbon pools of the northern mid- and high latitude forests. *Climatic Change*, **73**, pp. 355–368.

FRASER, C., HANLEY, H. and YAMAKAWA, T., 2002, High-precision geopositioning from IKONOS satellite imagery. In *Proceedings of ASPRS 2002 Conference*, 22–26 April 2002 (Washington, DC).

GRODECKI, J., 2001, IKONOS stereo feature extraction-RPC approach. In *Proceedings of ASPRS 2001 Conference*, 23–27 April 2001, St. Louis, MO.

HALBRITTER, K., 2000, Remote sensing for quantifying structural diversity in forests for forest biodiversity assessment. The research program BEAR: Indicators for Monitoring and Evaluation of Forest Biodiversity in Europe, *BEAR (European Union Project) Tech. Rep. No. 6*.

HELDER, D., COAN, M., PATRICK, K. and GASKA, P., 2003, IKONOS geometric characterization. *Remote Sensing of Environment*, **88**, pp. 69–79.

HU, Y., CROITORU, A. and TAO, V., 2004, Understanding the rational function model: methods and applications. In *International Archives of Photogrammetry and Remote Sensing*, 12–23 July 2004, Istanbul, vol. XX, pp. 119–124.

HYYPPÄ, J., KELLE, O., LEHIKOINEN, M. and INKINEN, M., 2001, A segmentation-based method to retrieve stem volume estimates from 3-D tree height models produced by laser scanners. *Transactions on Geoscience and Remote Sensing*, **39**, pp. 969–975.

KURZ, W.A. and APPS, M.J., 2006, Developing Canada's national forest carbon monitoring, accounting and reporting system to meet the reporting requirements of the Kyoto protocol. *Mitigation and Adaptation Strategies for Global Change*, **11**, pp. 33–43.

LAMBERT, M.-C., UNG, C.-H. and RAULIER, F., 2005, Canadian national tree aboveground equations. *Canadian Journal of Forest Research*, **35**, pp. 1996–2018.

LIM, K. and TREITZ, P., 2004, Estimation of above ground forest biomass from airborne discrete return laser scanner data using canopy-based quantile estimators. *Scandinavian Journal of Forest Research*, **19**, pp. 558–570.

LIM, K., TREITZ, P., BALDWIN, I., MORRISSON, J. and GREEN, J., 2003, Lidar remote sensing of biophysical properties of northern tolerant hardwood forests. *Canadian Journal of Remote Sensing*, **29**, pp. 2509–2525.

LIM, K., TREITZ, P., WULDER, M., ST-ONGE, B. and FLOOD, M., 2002, LiDAR remote sensing of forest structure. *Progress in Physical Geography*, **27**, pp. 88–106.

LU, D., 2005, Aboveground biomass estimation using Landsat Tm data in the Brazilian Amazon Basin. *International Journal of Remote Sensing*, **26**, pp. 2509–2525.

LU, D., 2006, The potential and challenge of remote sensing-based biomass estimation. *International Journal of Remote Sensing*, **27**, pp. 1297–1328.

MILLER, D.R., QUINE, C.P. and HADLEY, W., 2000, An investigation of the potential of digital photogrammetry to provide measurements of forest characteristics and abiotic damage. *Forest Ecology and Management*, **135**, pp. 279–288.

NÆSSET, E., 2002, Predicting forest stand characteristics with airborne scanning laser using a practical two-stage procedure and field data. *Remote Sensing of Environment*, **80**, pp. 88–99.

NOGUCHI, M., FRASER, C.S., NAKAMURA, T., SHIMONO, T. and OKI, S., 2004, Accuracy assessment of QuickBird stereo imagery. *The Photogrammetric Record*, **19**, pp. 128–137.

PATENAUDE, G., HILL, R.A., MILNE, R., GAVEAU, D.L.A., BRIGGS, B.B.J. and DAWSON, T., 2004, Quantifying forest above ground carbon contents using lidar remote sensing. *Remote Sensing of Environment*, **93**, pp. 368–380.

POON, J., FRASER, C., ZHANG, C., ZHANG, L. and GRUEN, A., 2005, Quality assessment of digital surface models generated from Ikonos imagery. *Photogrammetric Record*, **20**, pp. 162–171.

SANTOS, J.R., PARDI LACRUZ, M.S., ARAUJO, L.S. and KEIL, M., 2002, Savanna and tropical rainforest biomass estimation and spatialization using JERS-1 data. *International Journal of Remote Sensing*, **23**, pp. 1217–1229.

SPURR, S.H., 1960, *Photogrammetry and Photo-Interpretation* (New York: The Ronald Press Company).

STOKER, J.M., GREENLEE, S.K., GESCH, D.B. and MENIG, J.C., 2006, CLICK: The New USGS Center for Lidar Information Coordination and Knowledge. *Photogrammtric Engineering and Remote Sensing*, **72**, pp. 613–616.

ST-ONGE, B., JUMELET, J., COBELLO, M. and VÉGA, C., 2004, Measuring individual tree height using a combination of stereophotogrammetry and lidar. *Canadian Journal of Forest Research*, **34**, pp. 2122–2130.

ST-ONGE, B. and VÉGA, C., 2003, Combining stereo-photogrammetry and lidar to map forest canopy height. In *ISPRS Workshop on 3-D Reconstruction from Airborne Laser Scanner and InSAR Data*, October 2003, Dresden, Germany, pp. 205–210.

ST-ONGE, B., VEGA, C., FOURNIER, R. and HU, Y., 2007, Mapping canopy height using a combination of digital stereo-photogrammetry and lidar. *International Journal of Remote Sensing*, in press.

TOUTIN, T., 2003, Block bundle adjustment of Ikonos in-track images. *International Journal of Remote Sensing*, **24**, pp. 851–857.

TOUTIN, T., 2004, DSM generation and evaluation from QuickBird stereo imagery with 3D physical modelling. *International Journal of Remote Sensing*, **25**, pp. 5181–5192.

TREUHAFT, R.N. and SIQUEIRA, P.R., 2004, The calculated performance of forest structure and biomass estimates from interferometric radar. *Waves in Random Media*, **14**, pp. S345–S358.

ZAGALIKIS, G., CAMERON, A.D. and MILLER, D.R., 2005, The application of digital photogrammetry and image analysis techniques to derive tree and stand characteristics. *Canadian Journal of Forest Research*, **35**, pp. 1224–1237.

ZHANG, L., PATERAKI, M. and BALTSAVIAS, E., 2002, Matching of IKONOS stereo and multitemporal GEO images for DSM generation. In *Map Asia 2002*, Bangkok, CD-ROM.

ZHENG, D., RADEMACHER, J., CHEN, J., CROW, T., BRESEE, M., LE OINE, J. and RYU, S., 2004, Estimating above ground biomass using Landsat 7 ETM+ data across a managed landscape in northern Wisconsin. *Remote Sensing of Environment*, **93**, pp. 171–182.